Available online at www.sciencedirect.com

ScienceDirect

Proceedings of the Combustion Institute 000 (2020) 1–8

Proceedings of the Combustion Institute

www.elsevier.com/locate/proci

Experimental and numerical study of transcritical oxygen-hydrogen rocket flame response to transverse acoustic excitation

Scott K. Beinke [a,b], Justin S. Hardi [a,*], Daniel T. Banuti [c,d], Sebastian Karl [c], Bassam B. Dally [b], Michael Oschwald [a,e]

[a] *German Aerospace Center (DLR), Institute of Space Propulsion, Hardthausen 74239, Germany*
[b] *The University of Adelaide, South Australia 5005, Australia*
[c] *German Aerospace Center (DLR), Institute of Aerodynamics and Flow Technology, Göttingen 37073, Germany*
[d] *Department of Mechanical Engineering, The University of New Mexico, Albuquerque, NM 87114 USA*
[e] *Institute of Jet Propulsion and Turbomachinery, RWTH Aachen University, Aachen 52062, Germany*

Received 5 November 2019; accepted 29 May 2020
Available online xxx

Abstract

The response of a transcritical oxygen-hydrogen flame to transverse acoustic velocity was investigated using a combination of experimental analyses and numerical modelling. The experiment was conducted on a rectangular rocket combustor with shear coaxial injectors and continuously forced transverse acoustic field. Simultaneous high-speed shadowgraph and filtered OH* radiation images were collected and reduced using dynamic mode decomposition in order to characterise the flame response to the acoustic disturbance. CFD modelling of a representative single injector under forcing conditions was carried out to gain insights into the three-dimensional features of the reacting flow field. Invisible in the 2D projection, the model reveals that the excited LOX jet develops into a flattened and widened structure normal to the imposed acoustic velocity. The comparison of co-located structures allowed features in the imaging to be attributed to the deformation and transverse displacement of lower density oxygen surrounding the denser liquid oxygen core by the transverse acoustic velocity.

Keywords: Transcritical combustion; Rocket engine; Combustion instability

1. Introduction

High frequency combustion instability in liquid rocket engines (LREs) is not yet fully understood and concerted efforts are being invested to improve

---

* Corresponding author.
E-mail address: Justin.Hardi@dlr.de (J.S. Hardi).

https://doi.org/10.1016/j.proci.2020.05.027

Please cite this article as: S.K. Beinke, J.S. Hardi, D.T. Banuti et al., Experimental and numerical study of transcritical oxygen-hydrogen rocket flame response to transverse acoustic excitation, Proceedings of the Combustion Institute, https://doi.org/10.1016/j.proci.2020.05.027

its predictability in order to reduce the risk associated with developing new engines. Deeper understanding of the phenomenon may allow the development of improved methods for prevention and reduce the need for extensive ground testing of rocket propulsion systems. Fundamental research into the interaction between acoustic and combustion processes, in LRE combustion chambers, aims to understand the mechanisms which drive combustion instabilities. A key part of this research focuses on understanding how flames respond to acoustic disturbances in the combustion chamber leading to an unsteady heat release rate.

Several research groups have utilised sub-scale research combustors to subject flames to acoustic disturbances representative of high frequency combustion instabilities in rocket engines [1–5]. The extent of quantitative information gained from experiments to date is limited by the extent of optical access and other physical constraints on instrumentation. Thus, experimental insights into the processes contributing to the instabilities is correspondingly limited.

CFD modelling can potentially provide complementary information in order to better understand the flame response, and to capture the complex interplay of physical and chemical processes. Numerical simulations of acoustically driven flames under rocket combustion chamber conditions have been previously performed [4,6–8]. Large eddy simulation (LES) can capture the large scale flame dynamics and model the small scale. These models are computationally expensive and still face challenges in dealing with flows near the wall, capturing initial conditions, and resolving the interaction between turbulence and the reaction zone. Lower fidelity methods like URANS have the key advantage of a much lower computational cost. When validated, they likewise offer insights as research tools to complement measured data and to better understand the correlations between controlling parameters [9].

In the current study, an optically accessible combustor designated ‘BKH’ is used to conduct experiments [10]. BKH has tightly clustered shear-coaxial injection elements and is operated with supercritical (liquid) oxygen and hydrogen (LOX/H_2). In past work, the flame response to transverse acoustic forcing has been isolated by filtering or performing dynamic mode decomposition (DMD) on high-speed imaging of the flames [9,11]. However, interpretation of the complex features in the intensity distributions was incomplete due to a lack of understanding of their structure and dynamics. In literature in general one notes that the interpretation of 2D experimental results to date is based on 2D arguments. For example, the experimental results of Richecoeur [12] for transversally forced flames resulted in the purely 2D model of bulk heat release displacement. In the present work we provide added insight into the 3D nature of the flame response from 2D experimental imaging using 3D CFD modelling. The experiment and model cannot be treated separately because one is needed to understand the other.

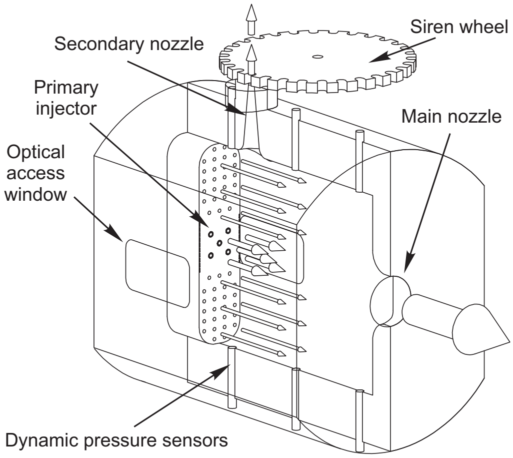

Fig. 1. Illustration of the BKH experiment.

In this paper, the BKH experimental data and DMD analysis are first presented. Then, computational results of a single injection element subjected to an acoustic disturbance using URANS are introduced. The model is then employed to identify and describe certain features of the DMD phase patterns that reflect a 3D flame response mechanism.

2. Experimental setup

The experimental rocket combustor model ‘H’ (‘BKH’) is depicted in Fig. 1. The combustion chamber features a rectangular geometry with windows located on each side for optical access to the near injector region, and a secondary nozzle and toothed wheel excitation system. The combustion chamber’s dimensions are 240 mm long, 50 mm wide and 200 mm high. Five shear coaxial injection elements are positioned in a matrix pattern in the middle of the chamber. The LOX and H_2 injectors have diameters of 3.5 and 5.8 mm (with slot width 0.55 mm), respectively.

During operation the toothed wheel is rotated at a controlled speed to modulate the flow through the secondary nozzle and cause an acoustic disturbance to propagate back into the chamber. The rectangular shaped internal volume was designed to deliberately fix the orientation of the first transverse (1T) acoustic mode and set its frequency to match those of upper-stage rocket engines, at around 4.4 kHz. High-frequency pressure measurements are recorded at various locations on the combustion chamber walls to resolve the acoustic field (a reconstruction of the 1T-mode acoustic field distribution is shown in Fig. S1).

Please cite this article as: S.K. Beinke, J.S. Hardi, D.T. Banuti et al., Experimental and numerical study of transcritical oxygen-hydrogen rocket flame response to transverse acoustic excitation, Proceedings of the Combustion Institute, https://doi.org/10.1016/j.proci.2020.05.027

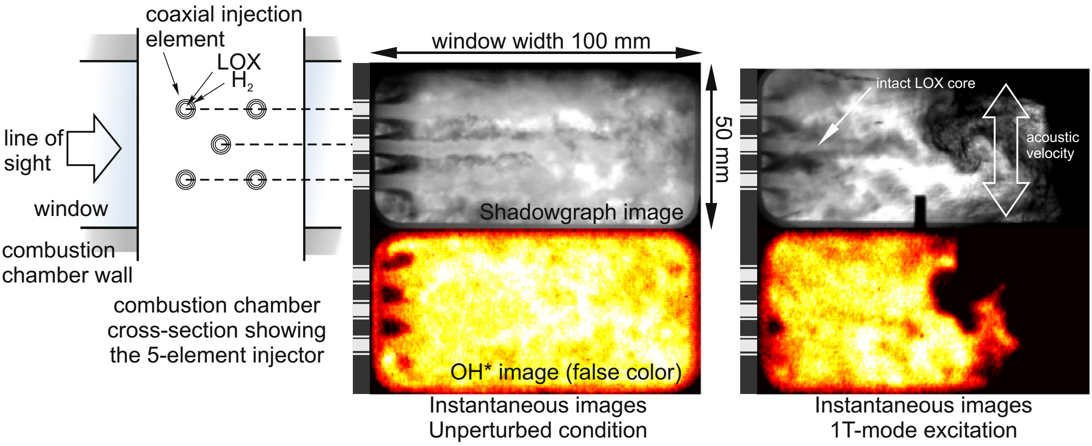

Fig. 2. Examples of instantaneous shadowgraph (upper row) and OH* radiation (lower row, false color) images in BKH, without (left) and with (right) 1T-mode forcing. (Movie: Fig. S2)

Additional information on BKH can be found in Refs [3,10,11]. The work presented here focuses on results for a single BKH operating point with a chamber pressure (P_{CC}) of 60 bar, and per-element injected mass flow rate of 113 g/s of LOX at 123 K and 19 g/s of H_2 at 288 K.

The optical diagnostics setup has previously been described by Hardi et al. [3,10]. The response of the injection elements to the acoustic disturbance is observed via simultaneous high-speed shadowgraph and filtered OH* radiation imaging captured through the optical access windows in the side walls of the chamber.

3. Experimental data analysis

Sample shadowgraph and OH* images, captured simultaneously, are shown in Fig. 2. On the left are instantaneous images from a test without active excitation system. Without external excitation, the combustor is always stable with pressure amplitude around 0.2% of P_{CC}. On the right are images during 1T-mode excitation with acoustic amplitude of 7.1% of P_{CC}. With the 1T mode, the transverse acoustic velocity increases mixing of the oxidiser and fuel streams and displaces the dense liquid oxygen core and surrounding flame zone.

A multi-variable DMD method was applied to identify coherent acoustic and optical intensity fluctuation at the transverse excitation frequency. The multi-variable DMD applies the same DMD method described by Schmid [13], but incorporates different types of measurements in the same calculation. Here, the pressure sensor data is synchronized and re-sampled to the imaging frame rate, then appended to the imaging matrix before processing the DMD. The shadowgraph and the OH* imaging were processed separately, but each with the same pressure data from the sensor indicated by the arrow in Fig. 1 By using the multi-variable DMD approach, the amplitude and phase relationship of the pressure data at the frequency of a particular optical DMD mode is retained. This has allowed the features in phase distributions from the optical imaging to be related to the acoustic cycle of the 1T mode at 4340 Hz.

3.1. *DMD results for flame-acoustic coupling*

The DMD mode from shadowgraph imaging during 1T-mode excitation, zoomed on the central injection element, is shown in Fig. 3a. The reconstructed shadowgraph image from the DMD mode is shown in the upper half and the phase relative to a sensor signal from the bottom wall of BKH is shown in the lower half. The phase distribution shows an alternating pattern of in and out of phase fluctuations across the height of the window region. This pattern is attributed to the vertical transport of the flame by the acoustic velocity. A pattern of alternating fluctuations, or ripples, on the surface of the LOX jet, are visible in both the reconstruction and phase distributions.

The corresponding DMD mode from the OH* data is shown in Fig. 3b. The fluctuations in the shear layer of the LOX stream that can be seen in the shadowgraph plots in Fig. 3a are not visible in the OH* distribution in Fig. 3b. At the high pressure and temperature encountered in BKH, UV radiation from OH* suffers high levels of self-absorption, and emission from thermally excited OH* exceeds chemiluminescence [14]. Consequently, in the line-of-sight images, the observer primarily sees the emission intensity of OH* from the outer most layers of the reacting flow field (thermally excited OH*) and only weakly through to

Please cite this article as: S.K. Beinke, J.S. Hardi, D.T. Banuti et al., Experimental and numerical study of transcritical oxygen-hydrogen rocket flame response to transverse acoustic excitation, Proceedings of the Combustion Institute, https://doi.org/10.1016/j.proci.2020.05.027

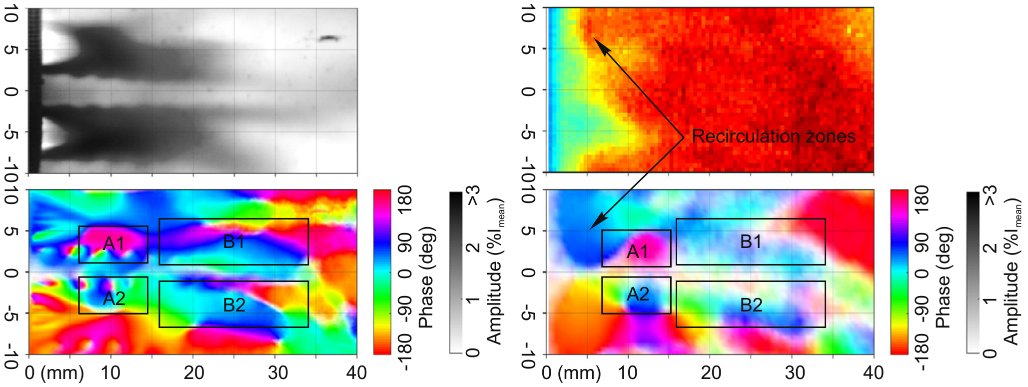

(a) Shadowgraph (b) OH*

Fig. 3. DMD mode reconstruction (above) and phase (below) for (a) the shadowgraph and (b) the OH* imaging. Phase is relative to pressure at the sensor on the bottom wall of BKH. The reconstruction is a snapshot from the cycle at phase 0. (Movie: Fig. S3)

the shear layer of the coaxial diffusion flame (OH chemiluminescence).

Viewing both the raw and reconstructed OH* movies (lower half of Figs. S2 and S3, respectively) gives the impression that the OH* field is entrained in the acoustic velocity field and oscillates vertically in a bulk sense. Therefore, the phase distribution in Fig. 3b largely describes the bulk vertical displacement of the low density, outer layers of the flame, most notable in the two large lobes from 0 to 10 mm describing the displacement of the recirculation zones of reaction products. The phase of these displacements is consistent with the downstream regions from 15 to 35 mm, labelled B1 and B2 in Fig. 3, which reflect the intensely reacting layers shed from the tip of the LOX core. This shows that radiation originating from the inner flame structure is still detectable through the blanketing outer layers.

Separating these regions is evidence of another inner flame structure effect; two distinct lobes appear on either side of the LOX core between 5 and 15 mm from the injection plane, labelled A1 and A2. These lobes lag the surrounding gas displacement by approximately 45°, or equivalently lead the bulk displacement on the opposite side of the LOX core. As will later become clear, this indicates local regions of lower density which are displaced differently to the bulk of the flame, and will be discussed later with respect to the CFD result.

4. Numerical method

4.1. CFD solver

An unsteady RANS approach with real-gas capability was used to model single injection elements under continuous acoustic forcing, approximating the conditions in the BKH experiment. We use the TAU Code, a hybrid grid, finite volume, compressible CFD solver developed by the German Aerospace Center (DLR) [15,16]. The code has been validated for various relevant cases, including transcritical combustion [17] and combustion instabilities [18].

We use the one-equation Spalart-Allmaras [19] turbulence model, Rossow's MAPS+ Riemann solver [20] with an explicit 3rd order Runge-Kutta scheme for time integration, and a second order Jameson-type dual time stepping scheme. The finite rate chemistry model uses Gaffney et al.'s [21] six-species (H_2, O_2, H, O, OH, H_2O) and seven-step reaction scheme for oxygen-hydrogen combustion.

To account for real-gas effects inside a high-pressure combustion chamber, the multi-fluid-mixing (MFM) model [17] is used. MFM is a thermodynamic zonal approach that solves a real fluid equation of state only where required. During transcritical LOX-GH_2 combustion, gases in the flame and hot reaction products behave as ideal gases [22]. Real fluid effects are confined to the LOX core and mixing occurs only after the oxygen transitions to an ideal gas state; i.e. mixing occurs essentially exclusively under ideal gas conditions [23]. Then, high-fidelity thermodynamic data for pure oxygen can be tabulated, resulting in ideal-gas cost during runtime for a Younglove's modified Benedict-Webb-Rubin equation [24] of state, rather than being limited to cubic equations of state. Real gas corrections to the transport coefficients are evaluated following Lemmon and Jacobsen [25]. Physically accurate, all flow outside of the dense core is treated as a mixture of ideal gases.

Please cite this article as: S.K. Beinke, J.S. Hardi, D.T. Banuti et al., Experimental and numerical study of transcritical oxygen-hydrogen rocket flame response to transverse acoustic excitation, Proceedings of the Combustion Institute, https://doi.org/10.1016/j.proci.2020.05.027

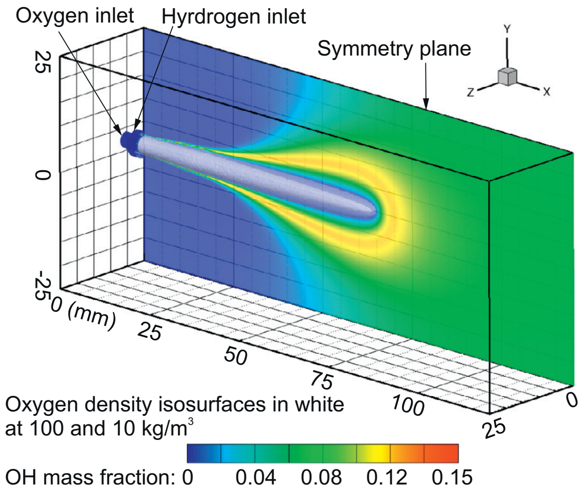

Fig. 4. Steady-state distribution of OH mass fraction and oxygen density isosurfaces overlaid on the domain used for 3D single-injector computations. (Movie: Fig. S4)

4.2. *Domain and boundary conditions*

The 3D numerical domain shown in Fig. 4 was employed to investigate the flame response to transverse acoustic velocity forcing. The domain includes the last few millimeters of the injector geometry connected to a larger volume representing part of the combustion chamber volume. The injector is located in a pressure node of the 1T mode and therefore has minimal coupling, so truncation was justified.

The modelled chamber volume is 120 mm long, 50 mm high, and 25 mm wide, with a symmetry plane dividing the flame. The dimensions of the 3D numerical domain were chosen in order to contain the flame from the single injection element while being sufficiently large that the flame does not intersect the side boundaries during transverse excitation.

The unstructured 3D mesh used approximately 590,000 nodes to fill the domain, with local refinement near the LOX post tip and in the shear layer between the LOX and H_2 streams. A grid refinement study has shown this is adequate for studying the flame distribution and LOX core dynamics for the chosen conditions.

Mass flow rate boundary conditions are specified at the oxygen and hydrogen inlets to match the experimental flow rate. All other surfaces, except the end of the domain, are specified as adiabatic viscous walls. To compute an initial steady-state RANS solution, a far-field condition is prescribed at the end boundary assuming an equilibrium mixture of combustion products at the desired chamber pressure.

For unsteady computations, the upper and lower boundaries of the computational subdomain of the chamber are treated with a periodically time-dependent near-field condition. In this flux-based condition, an outer state is prescribed and the boundary fluxes are calculated by means of an upwind scheme (AUSM). The outer state consists of the partial density distributions extrapolated from the resolved inner flow field, the prescribed periodic velocity field and the constant chamber pressure. In zones of local outflow from the computational domain, also the velocity field is extrapolated to the outer near-field state to ensure numerical consistency. As the local internal flow field state adapts to the modified far-field distribution, the acoustic disturbance is imposed upon the numerical domain.

5. Numerical results

5.1. *Steady-state results*

The single injector model was initialised by first computing a steady-state solution representing the unexcited flame. The steady-state solution shows the dense LOX core propagating into the centre of the domain and being enveloped by the flame, as indicated by the density isosurfaces and OH mass fraction distributions shown in Fig. 4. OH is a suitable marker for the structure of the reaction zone in high-pressure, diffusion dominated O_2-H_2 flames.

Further mesh refinement did not alter these distributions. The LOX core length compares well to the averaged core length measured from shadowgraph imaging under similar operating conditions (as reported in [3]), like that on the left side of Fig. 2 [18].

Please cite this article as: S.K. Beinke, J.S. Hardi, D.T. Banuti et al., Experimental and numerical study of transcritical oxygen-hydrogen rocket flame response to transverse acoustic excitation, Proceedings of the Combustion Institute, https://doi.org/10.1016/j.proci.2020.05.027

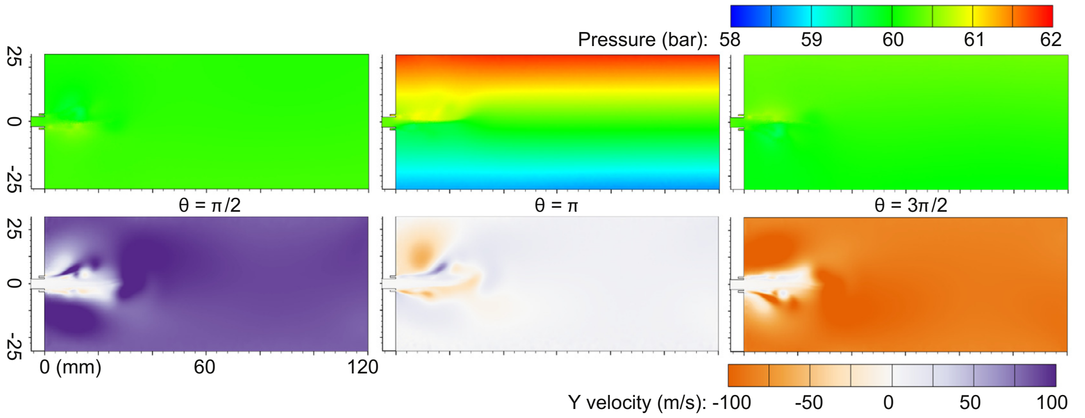

Fig. 5. Computed pressure and vertical velocity distributions during transverse excitation at different acoustic phase angles for 7.1% P_{CC} amplitude computation. (Movie: Fig. S5)

5.2. Unsteady results

The modulated boundary conditions were initiated for the unsteady computation which ran for 1000 time steps, or 22 acoustic cycles. A steady-state oscillatory condition was reached after about half this time (the first 16 cycles are shown in Fig. S4). The full duration required approximately 35,200 CPU hours on two 16 core AMD opteron 6274 processors to compute. Therefore the required resources were significantly less than in similar studies using LES which required millions of CPU hours to compute [6].

The excitation frequency and amplitude were chosen to match the experiment, with values of 4400 Hz and 7.1% of P_{CC}, respectively. Figure 5 shows the fluctuation of pressure and vertical velocity at the symmetry plane of the numerical domain at different phases of the acoustic cycle. The acoustic cycle is defined such that $\theta = 0$ corresponds to the peak pressure amplitude at the bottom surface of the domain.

The distributions in Fig. 5 shows that the imposed pressure disturbance produces the expected transverse gradient across the numerical domain. Similarly, the transverse Y velocity disturbance fluctuates with a $\pi/2$ phase shift relative to the imposed acoustic pressure disturbance. The velocity disturbance is almost uniform downstream, but is interrupted by the dense LOX core upstream, producing a complex velocity disturbance distribution in the near injector region.

The structure of the flame at phase angles of interest throughout an acoustic cycle was investigated using the 3D numerical results. Figures 6 and 7 show O_2 density and OH mass fraction iso-surfaces indicating the position of the LOX core and reaction front, respectively, at various phase angles once steady-state oscillation has been reached.

Consistent with LES results [6–8], we find that the acoustic velocity fluctuations deform the core and cause it to flatten in the plane normal to the imposed velocity. As the LOX core flattens it presents increasing surface area to the surrounding hydrogen stream and is more rapidly consumed, retracting towards the injection plane.

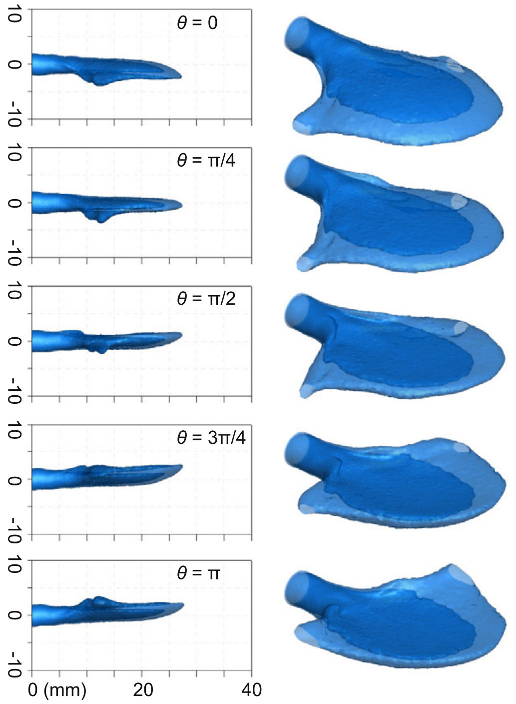

Fig. 6. Side and isometric views of oxygen density iso-surfaces of 10 and 50 kg/m^3 for different phase angles. (Movie: Fig. S6)

5.3. Flame dynamic response

Figure 8 shows the density distribution at the centre plane of the single injector model at the

Please cite this article as: S.K. Beinke, J.S. Hardi, D.T. Banuti et al., Experimental and numerical study of transcritical oxygen-hydrogen rocket flame response to transverse acoustic excitation, Proceedings of the Combustion Institute, https://doi.org/10.1016/j.proci.2020.05.027

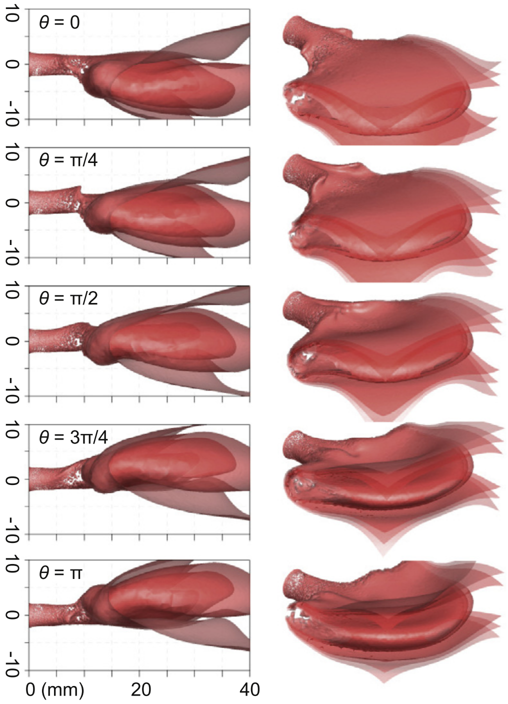

Fig. 7. Side and isometric views of OH mass fraction iso-surfaces of 0.06, 0.08, and 0.1 for different phase angles. (Movie: Fig. S7)

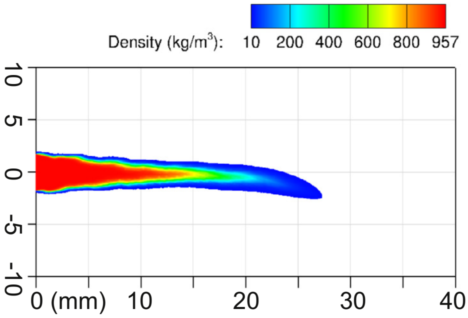

Fig. 8. CFD density distribution from a computation with 7.1% P_{CC} amplitude. Density shown with a cut-off value of 10 kg/m^3. (Movie: Fig. S8)

same phase of the acoustic cycle as the reconstructed shadowgraph image in Fig. 3. Both plots show wave-like structures alternating between the top and bottom surfaces of the LOX core. The crest and trough of each wave are similarly spaced along the length of the LOX core and become less pronounced downstream. These surface ripples are caused by the lighter outer layer of the dense core being transported by the acoustic velocity to one side of the LOX core upon entering the chamber, and then being convected downstream. As will become evident in the following discussion of Figs. 6 and 7, this combination of local and convective effects produces a travelling, rolling ridge, and this 3D topology appears as simple ripples when viewed in 2D profile as in Fig. 8.

The dynamics of the flame as seen in the CFD results in Figs. 6 and 7 will now be compared with the DMD phase distributions in Fig. 3. The sequences of images describe the vertical transport of the flame towards the top of the numerical domain by the transverse acoustic velocity from below.

Starting at a phase angle of $\theta = 0$, the flame has reached its maximum downward displacement from the previous acoustic cycle. The density iso-surfaces in Fig. 6 show the flattened LOX core deflected towards the bottom of the chamber.

By $\theta = \pi/4$, the acoustic velocity has begun to act on the flame from below, drawing protrusions from either side of the LOX core which are best seen in the isometric OH mass fraction iso-surface on the right side of Fig. 7. These protrusions have begun to roll up around the cylindrical core near the leading edge of the flattened 'wing'. This presents as a distinct ridge on top of the core in the side projection of the OH surface in Fig. 7 at around 10 mm downstream. The ridge occurs at the same coordinates as the region marked A1 in Fig. 3.

As the phase angle advances through $\theta = \pi/2$ to $3\pi/4$ the ridge begins to propagate outwards along the leading edges of the LOX wings. The lobes in the A regions in Fig. 3 appear to be co-located with this ridge. A1, for example, has a phase angle of approximately $\theta = 3\pi/4$ (magenta). This is consistent with an early shedding of reacting mixture from this ridge and the leading edge of the wings, ahead of the bulk displacement of the denser O_2 structure in Fig. 6. This means that these intensity lobes do not lie on the centre plane, but are somewhat in the foreground of the image, which could not be discerned from the planar imaging alone.

The rolling up and out motion of the ridges continues up to $\theta = \pi$ causing the leading outer edges of the flame, or the 'wing tips', to deflect further than some downstream sections, seen most clearly in the O_2 surface in Fig. 6. The regions marked B correspond to the vertical motion of the lighter gases about the flattened LOX core. The maximum displacement of this part of the flame is seen as bands at phase angles around $\theta = 0$ and π in the shadowgraph image in Fig. 3. From this the mean displacement of the flame is observed to be ± 5 mm about the central axis.

The B region features, in fact, have rolling phase leading up to π and beyond, but evident is a lag behind the radiation intensity peak in the A regions. The model describes the 3D structure of these features and explains the measured phase relationship between them.

Please cite this article as: S.K. Beinke, J.S. Hardi, D.T. Banuti et al., Experimental and numerical study of transcritical oxygen-hydrogen rocket flame response to transverse acoustic excitation, Proceedings of the Combustion Institute, https://doi.org/10.1016/j.proci.2020.05.027

6. Conclusions

The joint experimental and numerical analyses presented in this paper have identified phenomena important for understanding the response of coaxial, transcritical oxygen-hydrogen flames subjected to transverse acoustic forcing. Features of the dynamic flame response, such as lobes of lower density oxygen being transported by the acoustic velocity, and ripples on the surface of the oxygen core, were identified in 2D experimental datasets and explained by comparison with the 3D numerical results.

The flattening and flapping action of the flame explains the experimentally observed decrease in dense oxygen core length as the result of both its lateral redistribution and accelerated mixing with hydrogen.

While the deformation and displacement of the flame reproduced by the URANS model has been previously observed experimentally and predicted by others, the complementary analysis of imaging data presented here additionally related prominent features in the 2D experimental results to 3D mechanisms of the flame response.

Declaration of Competing Interest

None.

Acknowledgments

This work was conducted within the scope of the DLR Pro-Tau project and is also associated with the Franco-German Rocket Engine Stability iniTiative (REST). The authors would like to thank Bernd Wagner, Volker Hannemann, and Klaus Hannemann for their support with TAU, and Dmitry Suslov and the P8 test bench team for assistance operating BKH experiments. Research undertaken for this report has been assisted with a grant from the Sir Ross and Sir Keith Smith Fund (Smith Fund) (www.smithfund.org.au). The support is acknowledged and greatly appreciated.

Supplementary material

Supplementary material associated with this article can be found, in the online version, at doi:10.1016/j.proci.2020.05.027.

References

[1] F. Richecoeur, S. Ducruix, P. Scouflaire, S. Candel, *Proc. Combust. Inst.* 32 (2009) 1663–1670.
[2] M. Sliphorst, S. Gröning, M. Oschwald, *J. Propul. Power* 27 (2011) 182–189.
[3] J. Hardi, H.G. Martinez, M. Oschwald, *J. Propul. Power* 30 (2014) 337–349.
[4] C.J. Morgan, K.J. Shipley, W.E. Anderson, *J. Propul. Power* 31 (2015) 1696–1706.
[5] M. Roa, D.G. Talley, in: Proceedings of the AIAA Propulsion and Energy Forum, 2019.
[6] L. Hakim, A. Ruiz, T. Schmitt, M. Boileau, G. Staffelbach, S. Ducruix, B. Cuenot, S. Candel, *Proc. Combust. Inst.* 35 (2015) 1461–1468.
[7] L. Hakim, T. Schmitt, S. Ducruix, S. Candel, *Combust. Flame* 162 (2015) 3482–3502.
[8] A. Urbano, L. Selle, G. Staffelbach, B. Cuenot, T. Schmitt, S. Ducruix, S. Candel, *Combust. Flame* 169 (2016) 129–140.
[9] S. Beinke, D. Banuti, J. Hardi, M. Oschwald, B. Dally, in: Progress in Propulsion Physics, 11, EDP Sciences, 2019, pp. 225–246.
[10] J.S. Hardi, *Experimental investigation of high frequency combustion instability in cryogenic oxygen-hydrogen rocket engines*, The University of Adelaide, 2012 Ph.D. thesis.
[11] J.S. Hardi, S.K. Beinke, M. Oschwald, B.B. Dally, *J. Propul. Power* 30 (2014) 991–1004.
[12] F. Richecoeur, *Expérimentations et simulations numériques des interactions entre modes acoustiques transverses et flammes cryotechniques*, École Centrale Paris,, Paris, France, 2006 Ph.D. thesis.
[13] P.J. Schmid, *J. Fluid Mech.* 656 (2010) 528.
[14] T. Fiala, T. Sattelmayer, S. Gröning, J.S. Hardi, R. Stützer, S.C.L. Webster, M. Oschwald, *J. Propul. Power* 33 (2016) 490–500.
[15] D. Schwamborn, T. Gerhold, R. Heinrich, P. Wesseling, E. Onate, J. Périaux, in: Proceedings of the European Conference on Computational Fluid Dynamics (ECCOMAS CFD), 2006. TU Delft, The Netherlands
[16] S. Karl, *Numerical investigation of a generic scramjet configuration*, Technische Universität Dresden, 2011 Ph.D. thesis.
[17] D.T. Banuti, V. Hannemann, K. Hannemann, B. Weigand, *Combust. Flame* 168 (2016) 98–112.
[18] S. Beinke, *Analyses of flame response to acoustic forcing in a rocket combustor*, 2017 Ph.D. thesis. The University of Adelaide
[19] P. Spalart, S. Allmaras, in: Proceedings of the 30th AIAA Aerospace Sciences Meeting and Exhibit, 1992. Reno, NV
[20] C.C. Rossow, *AIAA J.* 41(12) (2003) 2379–2386.
[21] R.L. Gaffney, J.A. White, S.S. Girirnaji, J.P. Drummond, in: Proceedings of the AIAA/SAE/ASME/ASEE Joint Propulsion Conference and Exhibit, 1992. Nashville, TN
[22] G. Lacaze, J. Oefelein, *Combust. Flame* 159 (2012) 2087–2103.
[23] D.T. Banuti, P.C. Ma, J.-P. Hickey, M. Ihme, *Combust. Flame* 196 (2018) 364–376.
[24] B.A. Younglove, *J. Phys. Chem. Ref. Data* 11 (1982). Supplement No. 1
[25] E. Lemmon, R. Jacobsen, *Int. J. Thermophys.* 25(1) (2004) 21–69.

Please cite this article as: S.K. Beinke, J.S. Hardi, D.T. Banuti et al., Experimental and numerical study of transcritical oxygen-hydrogen rocket flame response to transverse acoustic excitation, Proceedings of the Combustion Institute, https://doi.org/10.1016/j.proci.2020.05.027